The Astrophysical Journal Letters, 891:L1 (9pp), 2020 March 1 https://doi.org/10.3847/2041-8213/ab75f0
© 2020. The American Astronomical Society. All rights reserved.

The Megamaser Cosmology Project. XIII. Combined Hubble Constant Constraints

D. W. Pesce[1,2], J. A. Braatz[3], M. J. Reid[1], A. G. Riess[4,5], D. Scolnic[6], J. J. Condon[3], F. Gao[3,7], C. Henkel[8,9], C. M. V. Impellizzeri[3,10], C. Y. Kuo[11,12], and K. Y. Lo[3,13]

[1] Center for Astrophysics | Harvard & Smithsonian, 60 Garden Street, Cambridge, MA 02138, USA; dpesce@cfa.harvard.edu
[2] Black Hole Initiative at Harvard University, 20 Garden Street, Cambridge, MA 02138, USA
[3] National Radio Astronomy Observatory, 520 Edgemont Road, Charlottesville, VA 22903, USA
[4] Department of Physics and Astronomy, Johns Hopkins University, Baltimore, MD, USA
[5] Space Telescope Science Institute, Baltimore, MD, USA
[6] Department of Physics, Duke University, 120 Science Drive, Durham, NC 27708, USA
[7] Key Laboratory for Research in Galaxies and Cosmology, Shanghai Astronomical Observatory, Chinese Academy of Science, Shanghai 200030, People's Republic of China
[8] Max-Planck-Institut für Radioastronomie, Auf dem Hügel 69, D-53121 Bonn, Germany
[9] Astronomy Department, Faculty of Science, King Abdulaziz University, P.O. Box 80203, Jeddah 21589, Saudi Arabia
[10] Joint ALMA Observatory, Alonso de Cordova 3107, Vitacura, Santiago, Chile
[11] Department of Physics, National Sun Yat-Sen University, No.70, Lianhai Rd., Gushan Dist., Kaohsiung City 804, Taiwan R.O.C.
[12] Academia Sinica Institute of Astronomy and Astrophysics, P.O. Box 23-141, Taipei 10617, Taiwan R.O.C.
Received 2020 January 24; revised 2020 February 7; accepted 2020 February 12; published 2020 February 26

Abstract

We present a measurement of the Hubble constant made using geometric distance measurements to megamaser-hosting galaxies. We have applied an improved approach for fitting maser data and obtained better distance estimates for four galaxies previously published by the Megamaser Cosmology Project: UGC 3789, NGC 6264, NGC 6323, and NGC 5765b. Combining these updated distance measurements with those for the maser galaxies CGCG 074-064 and NGC 4258, and assuming a fixed velocity uncertainty of 250 km s^{-1} associated with peculiar motions, we constrain the Hubble constant to be $H_0 = 73.9 \pm 3.0$ km s^{-1} Mpc^{-1} independent of distance ladders and the cosmic microwave background. This best value relies solely on maser-based distance and velocity measurements, and it does not use any peculiar velocity corrections. Different approaches for correcting peculiar velocities do not modify H_0 by more than $\pm 1\sigma$, with the full range of best-fit Hubble constant values spanning 71.8–76.9 km s^{-1} Mpc^{-1}. We corroborate prior indications that the local value of H_0 exceeds the early-universe value, with a confidence level varying from 95% to 99% for different treatments of the peculiar velocities.

Unified Astronomy Thesaurus concepts: Hubble constant (758); Observational cosmology (1146); Megamasers (1023); Water masers (1790); Very long baseline interferometry (1769)

1. Introduction

Ninety years after Hubble's seminal work (Hubble 1929), observational cosmology remains focused on obtaining a precise and accurate value of the Hubble constant, H_0. Today, measurements of the cosmic microwave background (CMB) at high redshift ($z \approx 1100$) determine the angular-size distance to the surface of last scattering, and within the context of the standard ΛCDM cosmological model, predict a precise value for H_0 of 67.4 ± 0.5 km s^{-1} Mpc^{-1} (Planck Collaboration et al. 2018). Because this "early-universe" prediction is model-dependent, complementary "late-universe" measurements of H_0 provide an important test of the assumed cosmological model (e.g., Hu 2005).

Currently, measurements of H_0 at low redshifts ($z \ll 10$) are in statistical tension with the early-universe prediction. For example, distance ladder measurements using Cepheid variables to calibrate the absolute luminosities of Type Ia supernovae find 74.03 ± 1.42 km s^{-1} Mpc^{-1} (Riess et al. 2019), and time-delay strong lensing measurements from multiply imaged quasars currently yield $73.3^{+1.7}_{-1.8}$ km s^{-1} Mpc^{-1} (Wong et al. 2019). Though this discrepancy between the early- and late-universe H_0 measurements is being taken increasingly seriously by the cosmological community (see Verde et al. 2019), the tantalizing prospects that it holds for heralding physics beyond ΛCDM (e.g., Raveri et al. 2017; Poulin et al. 2018) require that we subject it to a correspondingly strict evidence threshold. Independent avenues for constraining H_0 are thus necessary to provide cross-checks against unrecognized systematics in the measurements.

Water megamasers residing in the accretion disks around supermassive black holes (SMBHs) in active galactic nuclei (AGNs) provide a unique way to bypass the distance ladder and make one-step, geometric distance measurements to their host galaxies. The archetypal AGN accretion disk megamaser system is located in the nearby (7.6 Mpc; Humphreys et al. 2013; Reid et al. 2019) Seyfert 2 galaxy NGC 4258 (Claussen et al. 1984; Nakai et al. 1993; Herrnstein et al. 1999). Very long baseline interferometric (VLBI) observations reveal that the masers trace the accretion disk on sub-parsec scales, where the SMBH dominates the gravitational potential. The masing gas parcels act as test particles in this potential and exhibit the ordered, Keplerian motion expected for orbits about a point mass (Greenhill et al. 1995; Miyoshi et al. 1995). By combining the VLBI position and velocity information with centripetal accelerations measured from spectral monitoring observations (e.g., Argon et al. 2007), the typical degeneracy between mass and distance is broken and precise constraints can be placed on both quantities (e.g., Herrnstein et al. 1999; Humphreys et al. 2013; Reid et al. 2019).

The Megamaser Cosmology Project (MCP) is a multi-year campaign to find, monitor, and map AGN accretion disk megamaser systems (Braatz et al. 2007, 2008). The primary goal of the MCP is to constrain H_0 to a precision of several percent by making geometric distance measurements to megamaser galaxies

[13] Deceased.

in the Hubble flow (Kuo et al. 2013, 2015; Reid et al. 2013; Gao et al. 2017). Distance measurements made using the megamaser technique do not rely on distance ladders[14] or the CMB, and they have different systematics than lensing-based techniques. The megamaser measurements thus provide an independent handle on H_0.

In this paper we present a revised analysis that improves the distance measurements for several megamaser systems that have been previously published by the MCP. We then combine all distance measurements made using the revised analysis into a single megamaser-based constraint on H_0. The paper is organized as follows. In Section 2 we discuss the new disk modeling and compare our revised distance estimates with the previously published results. In Section 3 we describe how we combine the distance measurements into one H_0 constraint, detailing several different peculiar velocity treatments, and we present our resulting H_0 measurement. We summarize and conclude in Section 4.

2. Improved Distance Estimates

In this section we present updated distance measurements for the megamaser-hosting galaxies UGC 3789, NGC 6264, NGC 6323, and NGC 5765b. Each of these galaxies has had a maser-derived distance measurement published previously by the MCP (see Kuo et al. 2013, 2015; Reid et al. 2013; Gao et al. 2017).

The improvements we present here stem primarily from an update to the fitting procedure that incorporates the "error floor" systematic uncertainties as model parameters, thereby enabling marginalization over a previous source of systematic uncertainty. These error floors get added in quadrature with the data errors, such that an error floor value of zero indicates that the data errors already capture the true measurement uncertainties well. This updated model has already been applied to the galaxies NGC 4258 (Reid et al. 2019) and CGCG 074-064 (Pesce et al. 2020), so for these galaxies we simply use the corresponding published results.

We use a Hamiltonian Monte Carlo (HMC) sampler as implemented within the PyMC3 package (Salvatier et al. 2016) to perform all of the disk fitting described in this section; for a comprehensive overview of the disk model and fitting procedure, see Pesce et al. (2020). The HMC code yields results that match well with those from the Metropolis–Hastings disk-fitting code employed in many previous MCP publications (see, e.g., Reid et al. 2013), but has an improved convergence efficiency. We use broad truncated Gaussian priors for all error floor parameters, with a mean of 10 μas and a standard deviation of 5 μas for both the x- and y-position error floor priors, a mean of 2 km s^{-1} and a standard deviation of 1 km s^{-1} for both the systemic and high-velocity[15] error floor priors, and a mean of 0.3 km s^{-1} yr^{-1} and a standard deviation of 0.15 km s^{-1} yr^{-1} for the acceleration error floor priors. In all cases, the prior distribution is truncated at zero so that the error floors remain strictly positive.

Table 1
Results from Maser Disk Modeling

Galaxy	Distance (Mpc)	Velocity (km s^{-1})	Reference
UGC 3789	$51.5^{+4.5}_{-4.0}$	3319.9 ± 0.8	this work
NGC 6264	132.1^{+21}_{-17}	10192.6 ± 0.8	this work
NGC 6323	109.4^{+34}_{-23}	7801.5 ± 1.5	this work
NGC 5765b	$112.2^{+5.4}_{-5.1}$	8525.7 ± 0.7	this work
CGCG 074-064	$87.6^{+7.9}_{-7.2}$	7172.2 ± 1.9	Pesce et al. (2020)
NGC 4258	7.58 ± 0.11	679.3 ± 0.4	Reid et al. (2019)

Note. Maser galaxy distances and velocities as measured from modeling the maser disks; for each value we quote the posterior median and 1σ confidence interval (i.e., 16th to 84th percentile). For NGC 4258, where the systematic uncertainty in the distance measurement is comparable to its statistical uncertainty, we have added the two in quadrature. All velocities are quoted in the CMB reference frame using the optical convention. The values for the other parameters measured from the disk model are given in the Appendix.

2.1. UGC 3789

The disk megamaser in the galaxy UGC 3789 was discovered by Braatz & Gugliucci (2008), and the first VLBI map of the system was presented in Reid et al. (2009). This map was combined with acceleration measurements by Braatz et al. (2010) to produce an angular-size distance estimate of 49.9 ± 7.0 Mpc to the system. Reid et al. (2013) obtained additional data and improved the distance measurement to 49.6 ± 5.1 Mpc, and we use the data from that latest paper to produce the updated measurements presented in Table 1 and the Appendix.

Our updated fit indicates that the error floors used by Reid et al. (2013) for the position measurements were too conservative; we find a best-fit x-position error floor of 5 ± 1 μas and a best-fit y-position error floor of 6 ± 1 μas, compared to the previous (fixed) values of 10 μas for both x- and y-positions. We find that the data do not provide strong constraints on the velocity measurement error floors for either the systemic or the high-velocity masers, and that the posteriors for both largely follow the Gaussian-distributed prior range of 2.0 ± 1.0 km s^{-1}. Our best-fit acceleration error floor is 0.34 ± 0.06 km s^{-1} yr^{-1}, again indicating that the Reid et al. (2013) value of 0.57 km s^{-1} yr^{-1} was too conservative.

The net result of the updated modeling is a distance measurement of $D = 51.5^{+4.5}_{-4.0}$ Mpc, which represents a 3.8% ≈ 0.4σ increase over the previous value and an improvement in the measurement precision from ±10% to (+8.7%, −7.8%).

2.2. NGC 6264

A VLBI map for the maser system in NGC 6264 was first presented in Kuo et al. (2011), and Kuo et al. (2013) reported an angular-size distance measurement of 144 ± 19 Mpc. We use the data from the latter paper to produce the updated measurements in Table 1 and the Appendix.

[14] Though maser-based distances are independent of standard candle distances, we note that the reverse is not always true. There is one megamaser-hosting galaxy—NGC 4258—whose distance measurement has been used to anchor standard candle luminosity calibrations, potentially resulting in correlated uncertainties. However, Riess et al. (2019) find that H_0 measurements made using only the Large Magellanic Cloud and Milky Way parallaxes as calibration anchors (i.e., excluding the NGC 4258 calibration) yield results that are consistent with those that include the NGC 4258 calibration.

[15] Disk maser spectra are typically characterized by three groups of maser features arranged roughly symmetrically about the systemic velocity of the galaxy (see, e.g., Nakai et al. 1993; Braatz et al. 2004), corresponding to the locations in an edge-on accretion disk where the line-of-sight velocity gradient is minimized. The "systemic masers" sit in front of the black hole as seen along the line of sight, and in spectra they appear approximately centered on the systemic velocity of the system. The "high-velocity masers" originate on the "midline" of the disk (i.e., where the sky plane intersects the plane of the disk), where the line of sight passes tangent to the orbital velocity vectors, and in spectra they appear Doppler-shifted by typically several hundred km s^{-1} to either side of the systemic velocity.

Kuo et al. (2013) imposed error floors of 8 μas on the x-position measurements and 16 μas on the y-position measurements. We find that both of these values were too conservative; the updated fitting prefers x-position error floors that are consistent with zero and y-position error floors of 6 ± 2 μas. Our best-fit velocity error floors are only moderately constrained by the data (beyond the prior constraints); we find values of $1.6^{+0.9}_{-0.8}$ km s^{-1} and $1.3^{+0.7}_{-0.6}$ km s^{-1} for the systemic and high-velocity features, respectively, consistent with the error floors used in the previous disk modeling. We find that the acceleration error floor is consistent with zero and confined to a range of values that is considerably smaller than the $\sim$0.3–0.7 km s^{-1} yr^{-1} imposed on the measurements by Kuo et al. (2013).

The updated modeling yields an angular-size distance measurement of $D = 132.1^{+21}_{-17}$ Mpc, representing a $9\% \approx 0.6\sigma$ decrease compared to the previously published value. The uncertainty in the distance measurement remains essentially unchanged.

2.3. NGC 6323

The maser system in the galaxy NGC 6323 was discovered by Braatz et al. (2004), and the first VLBI map was presented in Braatz et al. (2007). Kuo et al. (2015) combined additional epochs of VLBI with spectral monitoring observations and reported an angular-size distance measurement of 107^{+42}_{-27} Mpc. We use the data from the latter paper to produce the updated measurements in Table 1 and the Appendix.

The original error floors in the position measurements were set to 10 μas, while we find that the updated disk modeling prefers a smaller value of 4 ± 1 μas for the x-positions and is consistent with zero for the y-positions. We find that the data are not able to place constraints on the velocity error floors, as our posteriors recover the prior Gaussian distributions of 2 ± 1 km s^{-1}. Our best-fit acceleration error floor is consistent with zero.

Our updated disk modeling constrains the distance to be $D = 109^{+34}_{-23}$ Mpc. This value matches well with the 107^{+42}_{-29} Mpc distance reported in Kuo et al. (2015), and we have improved the measurement precision from (+39%, −27%) to (+31%, −21%).

2.4. NGC 5765b

Gao et al. (2017) presented the maser system in NGC 5765b and measured its angular-size distance to be $122.0^{+10.0}_{-8.6}$ Mpc.[16] We use the data from that paper to produce the updated measurements in Table 1 and the Appendix.

We find that our disk fit prefers error floors of 3 ± 1 μas for both the x- and y-position data, indicating that the 10 μas error floors used in Gao et al. (2017) were too conservative. Conversely, we find the 0.6 km s^{-1} velocity error floors used in the original disk modeling were too optimistic, and the data place modest constraints on the velocity error floors of 1.1 ± 0.5 km s^{-1} and 1.5 ± 0.5 km s^{-1} for the systemic and high-velocity features, respectively. Our best-fit acceleration error floor of 0.04 ± 0.01 km s^{-1} yr^{-1} is on the low end of the 0.05–0.2 km s^{-1} yr^{-1} range used in Gao et al. (2017).

[16] Gao et al. (2017) reported a Hubble constant of 66.0 ± 5.0 Mpc using a recession velocity of 8334.6 km s^{-1}, which corresponds to a distance of $126.3^{+10.3}_{-8.9}$ Mpc using $D = v/H_0$. For this paper we convert between D and H_0 using Equation (1), so the distance of $122.0^{+10.0}_{-8.6}$ Mpc we mention here differs slightly from that reported in Gao et al. (2017).

Our updated disk modeling yields a distance measurement of $D = 112.2^{+5.4}_{-5.1}$ Mpc, a $9\% \approx 1\sigma$ decrease compared to the previously published value. The distance uncertainty has improved from (+8.2%, −7.0%) to (+4.8%, −4.5%).

3. Modeling the Hubble Constant

Our disk model returns an angular-size distance measurement $\hat{D}_i$ and a redshift measurement $\hat{z}_i$ for the SMBH in each megamaser-hosting galaxy. From considerations of kinetic energy equipartition between the SMBH and surrounding stars, we expect the relative velocity of a $\sim 10^7$ $M_\odot$ black hole to be $\ll 1$ km s^{-1} with respect to the system barycenter (Merritt et al. 2007). Measured upper limits on the magnitude of this relative motion are on the order of several km s^{-1} for the SMBH in the center of the Milky Way (Reid & Brunthaler 2004, 2020) and no more than a few tens of km s^{-1} for the sources considered in this work (Pesce et al. 2018). We thus proceed under the assumption that each galaxy effectively shares a distance and redshift with its SMBH, and we seek to determine what values of H_0 are compatible with these measurements.

For each galaxy, its expected angular-size distance D_i is related to its expected cosmological recession redshift z_i and H_0 by

$$D_i = \frac{c}{H_0(1+z_i)} \int_0^{z_i} \frac{dz}{\sqrt{\Omega_m(1+z)^3 + (1-\Omega_m)}} \approx \frac{cz_i}{H_0(1+z_i)} \left(1 - \frac{3\Omega_m z_i}{4} + \frac{\Omega_m(9\Omega_m - 4)z_i^2}{8}\right), \quad (1)$$

where by "expected" here we refer to the values that the distance and redshift would take if the galaxy were perfectly following the Hubble flow. Equation (1) assumes a flat ΛCDM cosmology, and the series expansion is accurate to one part in $\sim 10^5$ for the range of redshifts covered by our observations. We set $\Omega_m = 0.315$, from Planck Collaboration et al. (2018), though we note that any choice in the range $0 \leqslant \Omega_m \leqslant 0.5$ would yield a distance that differs by $\lesssim 1\%$ for the galaxies in our sample. For each of the H_0-fitting approaches described in this section, the contribution to the likelihood from the distance constraints is given by the product of the posterior distributions $\mathcal{P}(\hat{D}_i|D_i)$ from the independent disk fits,

$$\mathcal{L}_D = \prod_i \mathcal{P}(\hat{D}_i|D_i), \quad (2)$$

where $\hat{D}_i$ is the distance measured from disk modeling.

The expected cosmological recession velocity $v_i = cz_i$ differs from the measured galaxy velocity $\hat{v}_i$ both because of statistical uncertainty in the measurement and because of a systematic uncertainty in the form of peculiar motion. For our measurements, in which the statistical uncertainties in velocity are quite small (typically $\sim$1–2 km s^{-1}), peculiar motions dominate the recession velocity uncertainty. Because the galaxies in our sample all reside at low redshifts ($z \ll 1$), we proceed under the assumption that peculiar velocities are independent of redshift.

When fitting for H_0 we have several options for treating these peculiar velocities, and in this section we describe the

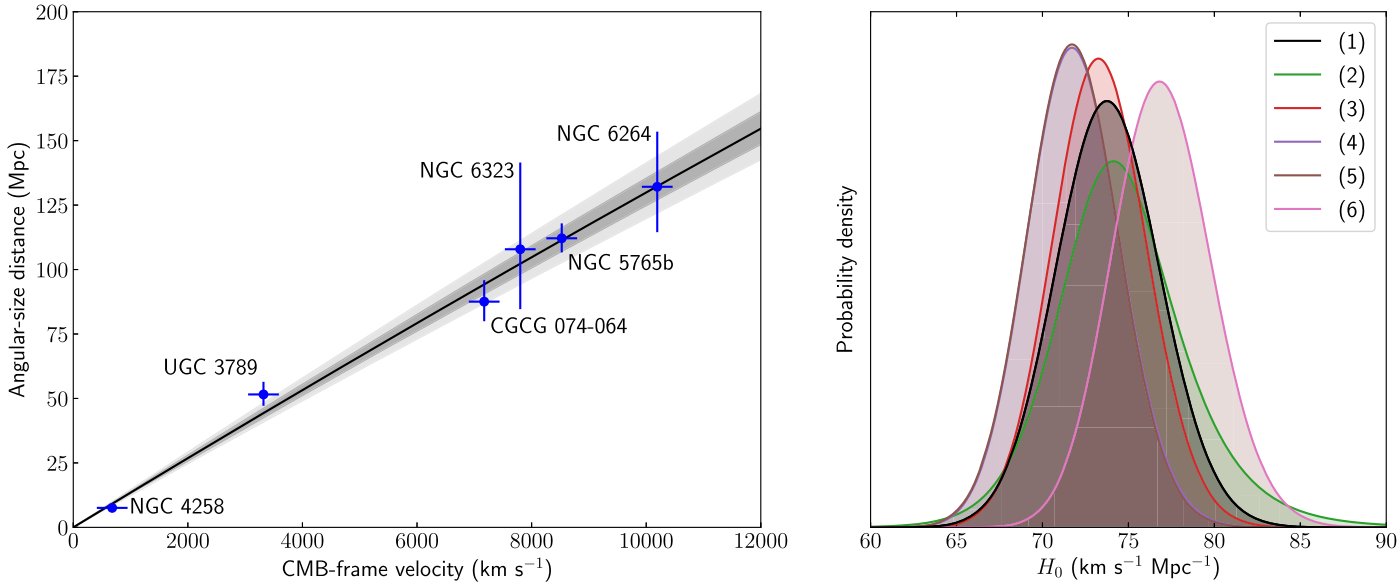

Figure 1. Left: Hubble diagram for the maser galaxies considered in this paper. Each data point is plotted with 1σ uncertainties in distance and 250 km s^{-1} uncertainties in velocity. The solid black line shows the distance–velocity relationship from Equation (1) for the maximum-likelihood H_0 value corresponding to the peculiar velocity treatment described in Section 3.1, and the shaded gray regions show 1σ and 2σ confidence intervals. Right: posterior distributions for H_0 from the five different peculiar velocity treatments considered in this paper; the treatments are numbered as in Table 2. Our "fiducial" treatment is (1) and is plotted in black. Note that treatments (4) and (5), corresponding to the galaxy flow corrections using 2M++ and CF3, return nearly identical H_0 posteriors.

approaches we have taken to construct the velocity contribution to the likelihood, $\mathcal{L}_v$. In all cases, our combined likelihood $\mathcal{L}$ is ultimately given by the product of the velocity and distance likelihoods,

$$\mathcal{L} = \mathcal{L}_D \mathcal{L}_v, \tag{3}$$

and the posterior distribution is given by the product of $\mathcal{L}$ with the prior via Bayes's theorem. We assume flat priors for all model parameters, and we explore the posterior space using the `dynesty` nested sampling package (Speagle 2020). The right panel of Figure 1 shows the posterior distributions for all model fits.

3.1. Treating Peculiar Velocities as Inflated Measurement Uncertainties

The simplest way to take peculiar velocities into account is to incorporate them into the velocity measurement uncertainties. Typical values for galaxy peculiar velocities lie in the range ∼150–250 km s^{-1} (e.g., Davis et al. 1997; Zaroubi et al. 2001; Masters et al. 2006; Hoffman et al. 2015), so we conservatively take the upper end of this range and add $\sigma_{\rm pec} = 250$ km s^{-1} in quadrature to our velocity uncertainties. The velocity contribution to the likelihood is then given by a Gaussian distribution,

$$\mathcal{L}_v = \prod_i \frac{1}{\sqrt{2\pi(\sigma_{v,i}^2 + \sigma_{\rm pec}^2)}} \exp\left(-\frac{1}{2}\frac{(v_i - \hat{v}_i)^2}{\sigma_{v,i}^2 + \sigma_{\rm pec}^2}\right), \tag{4}$$

where $\sigma_{v,i}$ is the statistical uncertainty in velocity measurement $\hat{v}_i$ and the true velocities v_i are treated as nuisance parameters in the model.

The result from fitting this model to all six maser galaxies simultaneously is $H_0 = 73.9 \pm 3.0$ km s^{-1} Mpc^{-1}, and Table 2 lists the values obtained from leave-one-out jackknife tests. We assess the goodness-of-fit using a chi-squared statistic,

$$\chi_\nu^2 = \frac{1}{\nu}\sum_i \left[\frac{(v_i - \hat{v}_i)^2}{\sigma_{v,i}^2 + \sigma_{\rm pec}^2} + \frac{(D_i - \hat{D}_i)^2}{\sigma_{D,i}^2}\right], \tag{5}$$

where $\sigma_{D,i}$ is the standard deviation of the distance measurement posterior and χ_ν^2 is the chi-squared per degree of freedom, ν. For this fit, $\nu = 5$ and $\chi_\nu^2 = 0.6$, which is consistent with unity within the expected standard deviation of a chi-squared distribution with five degrees of freedom (see also Table 3).

3.2. Modeling Peculiar Velocities as Being Drawn from a Global Distribution

Rather than assuming a typical dispersion for the peculiar velocity distribution of $\sigma_{\rm pec}$, we can instead fit for it as part of the model given some assumption about the form of the underlying distribution from which peculiar velocities are drawn. Because we expect that some unknown fraction of galaxies may have particularly large peculiar velocities (e.g., if the galaxy lives in a cluster), we test the (Sivia & Skilling 2006, Section 8.3.1) "conservative formulation" for the velocity uncertainties as an alternative to a Gaussian distribution. Under this formalism, $\sigma_{\rm pec}$ is interpreted as a lower bound on the velocity error σ associated with peculiar velocities, with a distribution for this error given by

$$\mathcal{P}(\sigma|\sigma_{\rm pec}) = \begin{cases} \dfrac{\sigma_{\rm pec}}{\sigma^2}, & \sigma > \sigma_{\rm pec} \\ 0, & \text{otherwise} \end{cases}. \tag{6}$$

The marginal likelihood contribution from the velocity constraints after integrating out σ is then

$$\mathcal{L}_v = \prod_i \frac{1}{\sqrt{2\pi(\sigma_{v,i}^2 + \sigma_{\rm pec}^2)}}\left(\frac{1 - e^{-R_i^2/2}}{R_i^2}\right), \tag{7}$$

Table 2
Hubble Constant Constraints and Jackknife Tests

Peculiar Velocity Treatment	Galaxies Excluded from the Fit	H_0 (km s^{-1} Mpc^{-1})
(1) Assign a fixed velocity uncertainty of 250 km s^{-1}	UGC 3789	$75.8^{+3.4}_{-3.3}$
	NGC 6264	$73.8^{+3.2}_{-3.2}$
	NGC 6323	$73.8^{+3.1}_{-3.0}$
	NGC 5765b	$74.1^{+4.5}_{-4.4}$
	CGCG 074-064	$72.5^{+3.4}_{-3.2}$
	NGC 4258	$73.6^{+3.1}_{-3.0}$
	Fit using all galaxies:	$73.9^{+3.0}_{-3.0}$
(2) Fit for $\sigma_{\rm pec}$ using the maser data and assuming an outlier-robust form for the peculiar velocity distribution	UGC 3789	$76.4^{+4.2}_{-3.8}$
	NGC 6264	$74.4^{+4.4}_{-3.8}$
	NGC 6323	$74.5^{+4.0}_{-3.6}$
	NGC 5765b	$75.8^{+6.6}_{-5.6}$
	CGCG 074-064	$73.1^{+4.3}_{-3.9}$
	NGC 4258	$74.2^{+4.5}_{-3.7}$
	Fit using all galaxies:	$74.4^{+3.9}_{-3.4}$
(3) Use galaxy group recession velocities	UGC 3789	$75.0^{+3.1}_{-3.0}$
	NGC 6264	$73.1^{+2.8}_{-2.7}$
	NGC 6323	$73.2^{+2.8}_{-2.7}$
	NGC 5765b	$72.2^{+4.2}_{-4.1}$
	CGCG 074-064	$73.3^{+3.1}_{-3.0}$
	NGC 4258	$72.8^{+2.8}_{-2.7}$
	Fit using all galaxies:	$73.3^{+2.8}_{-2.7}$
(4) Use 2M++ (Carrick et al. 2015) recession velocities	UGC 3789	$73.3^{+3.0}_{-3.0}$
	NGC 6264	$71.8^{+2.8}_{-2.8}$
	NGC 6323	$71.9^{+2.8}_{-2.7}$
	NGC 5765b	$71.1^{+4.0}_{-3.9}$
	CGCG 074-064	$70.9^{+3.0}_{-2.9}$
	NGC 4258	$72.1^{+2.7}_{-2.7}$
	Fit using all galaxies:	$71.8^{+2.7}_{-2.7}$
(5) Use CF3 (Graziani et al. 2019) recession velocities	UGC 3789	$73.6^{+3.1}_{-2.9}$
	NGC 6264	$71.5^{+2.8}_{-2.7}$
	NGC 6323	$71.7^{+2.8}_{-2.6}$
	NGC 5765b	$71.5^{+4.1}_{-4.0}$
	CGCG 074-064	$70.5^{+3.0}_{-2.9}$
	NGC 4258	$72.0^{+2.7}_{-2.7}$
	Fit using all galaxies:	$71.8^{+2.7}_{-2.6}$
(6) Use M2000 (Mould et al. 2000) recession velocities	UGC 3789	$79.3^{+3.3}_{-3.1}$
	NGC 6264	$76.8^{+2.9}_{-2.9}$
	NGC 6323	$76.9^{+2.9}_{-2.9}$
	NGC 5765b	$76.2^{+4.3}_{-4.1}$
	CGCG 074-064	$75.5^{+3.2}_{-3.0}$
	NGC 4258	$76.8^{+2.9}_{-2.9}$
	Fit using all galaxies:	$76.9^{+2.9}_{-2.9}$

Note. Hubble constant measurements made using various subsets of the megamaser distances and different treatments for the peculiar velocities, as described in Section 3. For each peculiar velocity treatment, we list seven H_0 values: six of these values correspond to "leave-one-out" jackknife tests, in which we fit the data (under the given peculiar velocity prescription) after removing the galaxy specified in the second column; the seventh value corresponds to that obtained from fitting all galaxies simultaneously. For each fit we quote the posterior median and 1σ confidence interval (i.e., 16th to 84th percentile).

where

$$R_i = \frac{v_{{\rm pec},i}^2}{\sigma_{v,i}^2 + \sigma_{\rm pec}^2}, \tag{8}$$

as we have assumed that the peculiar velocity distribution has zero mean.

Table 3
H_0 Goodnesses-of-fit and Comparisons with Other Measurements

Peculiar Velocity Treatment	χ_ν^2	$P(H_0 \leqslant H_{0,\rm Planck})$	$P(H_0 \geqslant H_{0,\rm SH0ES})$
(1)	0.60	0.02	0.48
(2)	1.52	0.03	0.55
(3)	0.62	0.01	0.41
(4)	0.55	0.05	0.24
(5)	0.75	0.05	0.23
(6)	0.75	<0.01	0.82

Note. Statistics for the Hubble constant fits described in Section 3, with the different peculiar velocity treatments numbered as in Table 2. The second column lists the chi-squared per degree of freedom for each fit, computed using Equation (5). For treatments (1), (3), (4), (5), and (6), the number of degrees of freedom $\nu = 5$ and the expected standard deviation of the χ_ν^2-distribution is $\sqrt{2/5} \approx 0.63$, while for treatment (2), $\nu = 4$ and the expected standard deviation in χ_ν^2 is $\sqrt{2/4} \approx 0.71$. The third column lists one-sided comparison statistics computed using Equation (10), which give the probability that our H_0 measurement is at least as low as the Planck measurement (Planck Collaboration et al. 2018). The fourth column is analogous to the third, and lists the probability that our H_0 measurement is at least as high as the SH0ES measurement (Riess et al. 2019; the statistic is computed using Equation (11)).

Because we are now modeling peculiar velocity rather than recession velocity, we have to relate the two. We relate the expected cosmological recession redshift z_i to the measured redshift $\hat{z}_i$ by adding the peculiar velocity contribution via (see, e.g., Davis & Scrimgeour 2014),

$$1 + \hat{z}_i = (1 + z_i)\left(1 + \frac{v_{{\rm pec},i}}{c}\right). \tag{9}$$

The z_i values are then plugged into Equation (1) to compute the distances D_i.

The result from fitting this model to all six maser galaxies simultaneously is $H_0 = 74.4^{+3.9}_{-3.4}$ km s^{-1} Mpc^{-1}, and Table 2 lists the values obtained from leave-one-out jackknife tests. We find $\sigma_{\rm pec} = 141^{+185}_{-80}$ km s^{-1} and use it via Equation (5) to compute $\chi_\nu^2 = 1.5$ (see Table 3), which is consistent with unity within the expected standard deviation for a chi-squared distribution with $\nu = 4$ degrees of freedom. We note also that the explicitly non-Gaussian form of the likelihood in Equation (7)—in particular the $1/R_i^2$ tails of this distribution—are expected to drive the chi-squared above unity.

3.3. Using Galaxy Group Velocities in Place of Individual Galaxy Velocities

As an alternative to treating the peculiar velocity as an uncertainty in the measured velocity, we can use external information to independently estimate the recession velocity for each galaxy in our sample. One of the primary drivers of peculiar motion is dispersion within galaxy groups or clusters, so we can attempt to correct for such dispersion by associating the cosmological recession velocity for each galaxy with the velocity of the group that galaxy resides in.

We use the galaxy groups defined in Tully (2015), and we take the velocities for the galaxies within each group from NED.[17] We define the group velocity to be the mean of all galaxy velocities

[17] The NASA/IPAC Extragalactic Database (NED) is funded by the National Aeronautics and Space Administration and operated by the California Institute of Technology.

Table 4
Relevant Velocities for Maser Galaxies

Galaxy	Velocity ($\mathrm{kms^{-1}}$)	Predicted Recession Velocity ($\mathrm{km\,s^{-1}}$)				Peculiar Velocity ($\mathrm{km\,s^{-1}}$)			
		Group	2M++	CF3	M2000	Group	2M++	CF3	M2000
UGC 3789	3319.9	3401	3375	3292	3464	−80	−54	28	−142
NGC 6264	10192.6	10379	9962	10175	10677	−180	224	17	−468
NGC 6323	7801.5	8275	7378	8112	8208	−461	414	−302	−396
NGC 5765b	8525.7	8594	8398	8333	9000	−66	124	187	−460
CGCG 074-064	7172.2	6511	6869	7037	7554	647	297	132	−372
NGC 4258	679.3	725	417	425	581	−46	262	254	98

Note. Various velocities relevant for the maser galaxies considered in this paper. The "velocity" column lists the CMB-frame velocity for the galaxy (defined such that $v = cz$) as measured from the maser disk fitting; we take this velocity to be a measure of the *actual* redshift of the galaxy with respect to us. The "predicted recession velocity" columns list the *expected* CMB-frame recession velocities for each galaxy (again defined such that $v = cz$) from one of two specified treatments; the group treatment is described in Section 3.3, and the 2M++ (Carrick et al. 2015)/CF3 (Graziani et al. 2019)/M2000 (Mould et al. 2000) treatment is described in Section 3.4. The CF3 recession velocities come courtesy of R. Graziani (2020, private communication). The "peculiar velocity" columns list the implied peculiar velocity for the galaxy, given the predicted and observed velocities. The peculiar velocity is defined via Equation (9), such that a positive value indicates that the galaxy has a larger redshift than would be predicted from purely Hubble flow motion.

within that group; these group recession velocities are listed in Table 4 along with their corresponding peculiar velocity equivalents. We note that not all of these group associations are equally certain, and that in particular the large peculiar velocity predicted for CGCG 074-064 (which was not associated with a galaxy group by Lavaux & Hudson 2011) may indicate that it warrants further investigation.

Given a recession velocity $\hat{v}_i$ for each galaxy group, we fit the model in the same manner described in Section 3.1, except we apply a $150\,\mathrm{km\,s^{-1}}$ rather than a $250\,\mathrm{km\,s^{-1}}$ global velocity uncertainty. We choose the low end of the plausible peculiar velocity range (see Section 3.1) because the galaxy groups, being much more massive than individual galaxies, should exhibit a smaller dispersion about the Hubble flow.

Fitting this model to all six maser galaxies simultaneously, we find $H_0 = 73.3^{+2.8}_{-2.7}\ \mathrm{km\,s^{-1}\,Mpc^{-1}}$. Table 2 lists the values obtained from leave-one-out jackknife tests for both models. We compute χ^2_ν using Equation (5) (see Table 3), and we find that the chi-squared values are consistent with unity within the expected standard deviation of a chi-squared distribution with $\nu = 5$ degrees of freedom.

3.4. Using Galaxy Flow Models to Correct for Peculiar Velocities

The last peculiar velocity treatment we consider is similar to the one described in the previous section in that it relies on the use of external information to constrain the permitted velocities for each galaxy in our sample. We obtain peculiar velocity predictions from three different galaxy flow models: (1) the "2M++ model" constructed by Carrick et al. (2015) using the 2M++ redshift catalog (Lavaux & Hudson 2011); (2) the "CF3 model" constructed by Graziani et al. (2019) from the *Cosmicflows-3* extragalactic distance database (Tully et al. 2016); and (3) the "M2000 model" constructed by Mould et al. (2000) to model the impact of the Great Attractor (GA), Virgo Cluster, and Shapley Cluster on galaxy motions. Each of these catalogs makes a prediction for the recession velocity associated with a particular sky direction and redshift, and we list these velocities in Table 4.

Given the recession velocity predictions from the catalogs, the model is fit in an identical manner to that used in Sections 3.1 and 3.3. We assume a $150\,\mathrm{km\,s^{-1}}$ uncertainty for all recession velocities, as per Carrick et al. (2015) for 2M++ and Graziani et al. (2019) for CF3.

Though each galaxy flow model makes different predictions for individual galaxy recession velocities (see Table 4), the results from fitting the 2M++ and CF3 models to all six maser galaxies simultaneously are in good agreement. We find $H_0 = 71.8 \pm 2.9\ \mathrm{km\,s^{-1}\,Mpc^{-1}}$ when using the 2M++ velocities and $H_0 = 71.8^{+2.7}_{-2.6}\ \mathrm{km\,s^{-1}\,Mpc^{-1}}$ for the CF3 velocities, both somewhat lower values than found using the treatments in previous sections.

For the M2000 model, we instead find a larger best-fit Hubble constant of $H_0 = 76.9 \pm 2.9\ \mathrm{km\,s^{-1}\,Mpc^{-1}}$. The M2000 model is simpler than either 2M++ or CF3 in that it considers only the gravitational influences of three large structures on individual galaxy motions, rather than using a global density field as done in both 2M++ and CF3. The substantial difference between the H_0 value predicted by the M2000 model and that predicted by the 2M++/CF3 models results from the effect of the GA in the M2000 infall model on three of the maser host galaxies. In the M2000 model, NGC 6264, NGC 5765b, and CGCG 074-064 are all in the direction of the GA and beyond it, reducing their perceived redshifts by our and their infall into the GA by 300–600 $\mathrm{km\,s^{-1}}$. These values get added back to the host galaxy velocities and thereby increase H_0. The veracity of these corrections is thus sensitive to the position and scale of the GA, which remains a subject of some debate (Dressler et al. 1987; Tully et al. 2014; Kraan-Korteweg et al. 2016; Hoffman et al. 2017).

Table 2 lists the H_0 values obtained from leave-one-out jackknife tests for each of the three models considered in this section, and Table 3 lists the χ^2_ν values computed using Equation (5). In all three cases we find that the χ^2_ν values are consistent with unity within the expected standard deviation of a chi-squared distribution with $\nu = 5$ degrees of freedom.

4. Summary and Discussion

We have applied an improved approach for fitting maser data to obtain more precise distance estimates to four previously published MCP galaxies: UGC 3789, NGC 6264, NGC 6323, and NGC 5765b. We find that previous maser disk modeling efforts have typically overestimated the systematic measurement

uncertainties associated with maser positions from VLBI maps. By incorporating these error floors into our disk model as model parameters, we are able to fit for and then marginalize over them, eliminating a source of systematic uncertainty and generically improving the measurement precision. We have combined the revised distance estimates for UGC 3789, NGC 6264, NGC 6323, and NGC 5765b with the recently published distances to CGCG 074-064 and NGC 4258—both of which included error floors as parameters in the model—to derive constraints on H_0. Assuming a global velocity uncertainty of 250 km s^{-1} associated with peculiar motions, we find $H_0 = 73.9 \pm 3.0$ km s^{-1} Mpc^{-1}. A Hubble diagram is shown in the left panel of Figure 1.

Our fiducial H_0 measurement is determined exclusively using megamaser-based distance and velocity measurements, and it thus represents an independent cosmological probe from standard candles, gravitational lenses, and the CMB. The primary source of systematic uncertainty in this measurement comes from the unknown peculiar motions of the maser galaxies, and we have considered three different treatments[18] for determining how these peculiar velocities could modify the H_0 value:

1. We permit the global velocity uncertainty to be a free parameter that we fit alongside H_0.
2. We replace each galaxy's recession velocity with the velocity of the group that galaxy is a member of.
3. We replace each galaxy's recession velocity with the velocity predicted by a galaxy flow model evaluated at that galaxy's location and redshift. We use the 2M++, CF3, and M2000 peculiar velocity models.

The first two of the above treatments modify the best-fit H_0 value by less than 1 km s^{-1} Mpc^{-1}, though the measurement precision suffers when permitting the global velocity uncertainty to be a free parameter because of the reduced degrees of freedom. Using recession velocities from either the 2M++ or CF3 galaxy flow models systematically reduces the best-fit H_0 value by 2.1 km s^{-1} Mpc^{-1}, and the measurement precision improves because of the smaller uncertainty (150 km s^{-1}) associated with the catalog velocities. The recession velocities from the M2000 model, on the other hand, result in a substantially increased best-fit H_0 value, which is larger by 3.0 km s^{-1} Mpc^{-1} than the fiducial measurement and by 5.1 km s^{-1} Mpc^{-1} than the measurement made from correcting for peculiar velocities using the other two flow models.

We have also performed a series of leave-one-out jackknife tests for each of the different peculiar velocity treatments. We find that the removal of any single galaxy from the sample never modifies the best-fit H_0 value by more than 1σ, indicating that our measurement is not being unduly influenced by a single outlying value.

We test the prior empirical claim that the local value of H_0 exceeds the early-universe value (e.g., Riess et al. 2019; Verde et al. 2019; Wong et al. 2019) by calculating the probability of rejecting the null hypothesis that our measurement does not exceed Planck's, i.e.,

$$P(H_0 \leqslant H_{0,\mathrm{Planck}}) = \int_{-\infty}^{\infty} \mathcal{P}(H)\left[\int_{-\infty}^{H} \mathcal{P}(H_0')dH_0'\right]dH, \quad (10)$$

where $\mathcal{P}(H_0)$ is our measured posterior distribution for H_0 and we treat the Planck measurement probability distribution $\mathcal{P}(H)$ as a Gaussian with mean and standard deviation given by the published measurement of $H_{0,\mathrm{Planck}} = 67.4 \pm 0.5$ km s^{-1} Mpc^{-1} (Planck Collaboration et al. 2018). The value of $P(H_0 \leqslant H_{0,\mathrm{Planck}})$ is listed for all four peculiar velocity treatments in Table 3. The first treatment, our default, gives a 2% chance that our value is lower than Planck's, corroborating the sense of the present tension in H_0 at 98% confidence. The other peculiar velocity treatments give confidences of 95%–99%. Performing an analogous comparison with a late-universe measurement from SH0ES of $H_{0,\mathrm{SH0ES}} = 74.03 \pm 1.42$ km s^{-1} Mpc^{-1} (Riess et al. 2019),

$$P(H_0 \geqslant H_{0,\mathrm{SH0ES}}) = \int_{-\infty}^{\infty} \mathcal{P}(H)\left[\int_{H}^{\infty} \mathcal{P}(H_0')dH_0'\right]dH, \quad (11)$$

we find that our result is consistent with the SH0ES measurement, with little preference for a higher or lower value (see Table 3).

The ~4% H_0 constraint presented in this paper comes from consideration of only six megamaser-hosting galaxies, and the precision is ultimately limited by the quality and quantity of the available distance measurements. Future H_0 measurements from the MCP will improve on this precision by incorporating distance measurements from additional megamaser-hosting galaxies.

We thank R. B. Tully and R. Graziani for help with the *Cosmicflows-3* peculiar velocities, M. J. Hudson for advice regarding the 2M++ peculiar velocities, L. Blackburn for modeling discussions, and Erik Peterson for help with understanding redshift uncertainties. The National Radio Astronomy Observatory is a facility of the National Science Foundation operated under cooperative agreement by Associated Universities, Inc. This work made use of the Swinburne University of Technology software correlator, developed as part of the Australian Major National Research Facilities Programme and operated under license. This research has made use of the NASA/IPAC Extragalactic Database (NED), which is operated by the Jet Propulsion Laboratory, California Institute of Technology, under contract with the National Aeronautics and Space Administration. This work was supported in part by the black hole Initiative at Harvard University, which is funded by grants from the John Templeton Foundation and the Gordon and Betty Moore Foundation to Harvard University.

Facilities: GBT, VLA, VLBA, Effelsberg.

Software: AIPS, CASA, GBTIDL, PyMC3 (Salvatier et al. 2016), `dynesty` (Speagle 2020).

Appendix
Updated Disk Modeling Parameter Values

In Table 5 we list the values for all model parameters from the updated disk fits to UGC 3789, NGC 6264, NGC 6323, and NGC 5765b. A comprehensive description of the model is given in Pesce et al. (2020).

[18] We note that a variety of peculiar velocity correction schemes are possible beyond what we have explicitly tested in this paper, including compound schemes that combine two or more of the above methods.

Table 5
Updated Disk-fitting Results

Parameter	Units	Galaxy			
		UGC 3789	NGC 6264	NGC 6323	NGC 5765b
D	Mpc	$51.5^{+4.5}_{-4.0}$	$132.1^{+21.2}_{-17.3}$	$109.4^{+34.2}_{-23.4}$	$112.2^{+5.4}_{-5.1}$
$M_{\rm BH}$	$10^7\ M_\odot$	$1.19^{+0.10}_{-0.09}$	$2.76^{+0.45}_{-0.36}$	$1.02^{+0.32}_{-0.22}$	$4.15^{+0.20}_{-0.19}$
v	km s^{-1}	3319.9 ± 0.8	10192.6 ± 0.8	7801.5 ± 1.5	8525.7 ± 0.7
x_0	mas	-0.4014 ± 0.0010	0.0050 ± 0.0012	0.0161 ± 0.0010	-0.0440 ± 0.0014
y_0	mas	-0.4615 ± 0.0011	0.0076 ± 0.0016	0.0073 ± 0.0024	-0.0995 ± 0.0019
i_0	degree	84.9 ± 0.6	91.3 ± 2.3	91.5 ± 0.3	72.4 ± 0.5
$\frac{di}{dr}$	degree mas^{-1}	7.7 ± 1.0	-1.5 ± 4.0	…	12.5 ± 0.5
Ω_0	degree	222.4 ± 0.4	84.7 ± 1.3	184.4 ± 0.6	149.7 ± 0.3
$\frac{d\Omega}{dr}$	degree mas^{-1}	-1.6 ± 0.6	16.7 ± 2.2	12.9 ± 1.2	-3.2 ± 0.2
σ_x	mas	0.0045 ± 0.0011	$0.0012^{+0.0011}_{-0.0008}$	0.0035 ± 0.0010	$0.0028^{+0.0012}_{-0.0011}$
σ_y	mas	0.0063 ± 0.0013	0.0056 ± 0.0020	$0.0037^{+0.0025}_{-0.0022}$	0.0034 ± 0.0009
$\sigma_{v,\rm sys}$	km s^{-1}	$1.7^{+0.9}_{-0.8}$	$1.6^{+0.9}_{-0.8}$	$2.1^{+1.0}_{-0.9}$	1.1 ± 0.5
$\sigma_{v,\rm hv}$	km s^{-1}	$1.8^{+0.9}_{-0.7}$	$1.3^{+0.7}_{-0.6}$	$1.9^{+0.9}_{-0.7}$	$1.5^{+0.6}_{-0.5}$
σ_a	km s^{-1} yr^{-1}	$0.34^{+0.06}_{-0.05}$	$0.08^{+0.07}_{-0.05}$	0.21 ± 0.09	0.041 ± 0.014

Note. Top: fitting results for the global parameters describing the maser disk, marginalized over all other parameters; for each value we quote the posterior median and 1σ confidence interval (i.e., 16th to 84th percentile). Here, D is the angular-size distance to the galaxy, $M_{\rm BH}$ is the mass of the SMBH, v is the line-of-sight CMB-frame velocity of the SMBH, (x_0, y_0) is the coordinate location of the SMBH, i_0 is the inclination angle of the disk at $r = 0$, $\frac{di}{dr}$ is the first-order inclination angle warping parameter, Ω_0 is the position angle of the disk at $r = 0$, and $\frac{d\Omega}{dr}$ is the first-order position angle warping parameter. For the uncertainties we quote 1σ (i.e., 16% and 84%) confidence intervals from the posteriors. The SMBH coordinate locations are referenced to the coordinate zero-point used in the respective data paper: for UGC 3789, see Reid et al. (2009); for NGC 6264, see Kuo et al. (2013); for NGC 6323, see Kuo et al. (2015); and for NGC 5765b, see Gao et al. (2017). Bottom: fitting results for the error floor parameters; σ_x is the x-position error floor, σ_y is the y-position error floor, $\sigma_{v,\rm sys}$ is the error floor for the systemic feature velocities, $\sigma_{v,\rm hv}$ is the error floor for the high-velocity feature velocities, and σ_a is the acceleration error floor.

ORCID iDs

D. W. Pesce https://orcid.org/0000-0002-5278-9221
J. A. Braatz https://orcid.org/0000-0002-1468-9203
M. J. Reid https://orcid.org/0000-0001-7223-754X
J. J. Condon https://orcid.org/0000-0003-4724-1939
F. Gao https://orcid.org/0000-0002-2581-9114
C. Henkel https://orcid.org/0000-0002-7495-4005
C. M. V. Impellizzeri https://orcid.org/0000-0002-3443-2472
C. Y. Kuo https://orcid.org/0000-0001-6211-5581

References

Argon, A. L., Greenhill, L. J., Reid, M. J., Moran, J. M., & Humphreys, E. M. L. 2007, ApJ, 659, 1040
Braatz, J., Greenhill, L., Reid, M., et al. 2007, in IAU Symp. 242, Astrophysical Masers and their Environments, ed. J. M. Chapman & W. A. Baan (Cambridge: Cambridge Univ. Press), 399
Braatz, J. A., & Gugliucci, N. E. 2008, ApJ, 678, 96
Braatz, J. A., Henkel, C., Greenhill, L. J., Moran, J. M., & Wilson, A. S. 2004, ApJL, 617, L29
Braatz, J. A., Reid, M. J., Greenhill, L. J., et al. 2008, in ASP Conf. Ser. 395, Investigating Dark Energy with Observations of H2O Megamasers, ed. A. H. Bridle, J. J. Condon, & G. C. Hunt (San Francisco, CA: ASP), 103
Braatz, J. A., Reid, M. J., Humphreys, E. M. L., et al. 2010, ApJ, 718, 657
Carrick, J., Turnbull, S. J., Lavaux, G., & Hudson, M. J. 2015, MNRAS, 450, 317
Claussen, M. J., Heiligman, G. M., & Lo, K. Y. 1984, Natur, 310, 298
Davis, M., Miller, A., & White, S. D. M. 1997, ApJ, 490, 63
Davis, T. M., & Scrimgeour, M. I. 2014, MNRAS, 442, 1117
Dressler, A., Faber, S. M., Burstein, D., et al. 1987, ApJL, 313, L37
Gao, F., Braatz, J. A., Reid, M. J., et al. 2017, ApJ, 834, 52
Graziani, R., Courtois, H. M., Lavaux, G., et al. 2019, MNRAS, 488, 5438
Greenhill, L. J., Jiang, D. R., Moran, J. M., et al. 1995, ApJ, 440, 619
Herrnstein, J. R., Moran, J. M., Greenhill, L. J., et al. 1999, Natur, 400 539
Hoffman, Y., Courtois, H. M., & Tully, R. B. 2015, MNRAS, 449, 4494
Hoffman, Y., Pomarède, D., Tully, R. B., & Courtois, H. M. 2017, NatAs, 1, 0036
Hu, W. 2005, in ASP Conf. Ser. 339, Dark Energy Probes in Light of the CMB, ed. S. C. Wolff & T. R. Lauer (San Francisco, CA: ASP), 215
Hubble, E. 1929, PNAS, 15, 168
Humphreys, E. M. L., Reid, M. J., Moran, J. M., Greenhill, L. J., & Argon, A. L. 2013, ApJ, 775, 13
Kraan-Korteweg, R. C., Elson, E., Blyth, S., et al. 2016, Proceedings of MeerKAT Science: On the Pathway to the SKA (MeerKAT2016) (Trieste: SISSA), 21
Kuo, C. Y., Braatz, J. A., Condon, J. J., et al. 2011, ApJ, 727, 20
Kuo, C. Y., Braatz, J. A., Lo, K. Y., et al. 2015, ApJ, 800, 26
Kuo, C. Y., Braatz, J. A., Reid, M. J., et al. 2013, ApJ, 767, 155
Lavaux, G., & Hudson, M. J. 2011, MNRAS, 416, 2840
Masters, K. L., Springob, C. M., Haynes, M. P., & Giovanelli, R. 2006, ApJ, 653, 861
Merritt, D., Berczik, P., & Laun, F. 2007, AJ, 133, 553
Miyoshi, M., Moran, J., Herrnstein, J., et al. 1995, Natur, 373, 127
Mould, J. R., Huchra, J. P., Freedman, W. L., et al. 2000, ApJ, 529, 786
Nakai, N., Inoue, M., & Miyoshi, M. 1993, Natur, 361, 45
Pesce, D. W., Braatz, J. A., Condon, J. J., & Greene, J. E. 2018, ApJ, 863 149
Pesce, D. W., Braatz, J. A., Reid, M. J., et al. 2020, arXiv:2001.04581
Planck Collaboration, Aghanim, N., Akrami, Y., et al. 2018, arXiv:1807.06209
Poulin, V., Boddy, K. K., Bird, S., & Kamionkowski, M. 2018, PhRvD, 97, 123504
Raveri, M., Hu, W., Hoffman, T., & Wang, L.-T. 2017, PhRvD, 96, 103501
Reid, M. J., Braatz, J. A., Condon, J. J., et al. 2009, ApJ, 695, 287
Reid, M. J., Braatz, J. A., Condon, J. J., et al. 2013, ApJ, 767, 154
Reid, M. J., & Brunthaler, A. 2004, ApJ, 616, 872
Reid, M. J., & Brunthaler, A. 2020, arXiv:2001.04386
Reid, M. J., Pesce, D. W., & Riess, A. G. 2019, ApJL, 886, L27
Riess, A. G., Casertano, S., Yuan, W., Macri, L. M., & Scolnic, D. 2019, ApJ, 876, 85

Salvatier, J., Wiecki, T. V., & Fonnesbeck, C. 2016, PeerJ Comput. Sci., 2, e55
Sivia, D., & Skilling, J. 2006, Data Analysis: A Bayesian Tutorial (Oxford: Oxford Univ. Press)
Speagle, J. S. 2020, MNRAS, in press (doi:10.1093/mnras/staa278)
Tully, R. B. 2015, AJ, 149, 171
Tully, R. B., Courtois, H., Hoffman, Y., & Pomarède, D. 2014, Natur, 513, 71
Tully, R. B., Courtois, H. M., & Sorce, J. G. 2016, AJ, 152, 50
Verde, L., Treu, T., & Riess, A. G. 2019, NatAs, 3, 891
Wong, K. C., Suyu, S. H., Chen, G. C. F., et al. 2019, arXiv:1907.04869
Zaroubi, S., Bernardi, M., da Costa, L. N., et al. 2001, MNRAS, 326, 375